THE JOURNAL OF BIOLOGICAL CHEMISTRY VOL. 287, NO. 1, pp. 660–671, January 2, 2012

Angiotensin II Increases Activity of the Epithelial Na^+ Channel (ENaC) in Distal Nephron Additively to Aldosterone*

Received for publication, August 29, 2011, and in revised form, November 14, 2011 Published, JBC Papers in Press, November 15, 2011, DOI 10.1074/jbc.M111.298919

Mykola Mamenko[‡1], **Oleg Zaika**[‡1], **Daria V. Ilatovskaya**[§¶], **Alexander Staruschenko**[§], **and Oleh Pochynyuk**[‡2]

From the [‡]*Department of Integrative Biology and Pharmacology, the University of Texas Health Science Center, Houston, Texas 77030, the* [§]*Department of Physiology, Medical College of Wisconsin, Milwaukee, Wisconsin 53226, and the* [¶]*Institute of Cytology, Russian Academy of Sciences, 194064 St. Petersburg, Russia*

Background: Mineralocorticoid aldosterone controls ENaC-mediated Na^+ reabsorption in the distal nephron.
Results: Ang II stimulates production of reactive oxygen species to stimulate ENaC, and this effect is preserved when mineralocorticoids are high.
Conclusion: Ang II directly controls ENaC activity and expression in murine distal nephrons.
Significance: Ang II may have a specific role in regulation of sodium handling in the distal nephron during variations in dietary Na^+ intake.

Dietary salt intake controls epithelial Na^+ channel (ENaC)-mediated Na^+ reabsorption in the distal nephron by affecting status of the renin-angiotensin-aldosterone system (RAAS). Whereas regulation of ENaC by aldosterone is generally accepted, little is known about whether other components of RAAS, such as angiotensin II (Ang II), have nonredundant to aldosterone-stimulatory actions on ENaC. We combined patch clamp electrophysiology and immunohistochemistry in freshly isolated split-opened distal nephrons of mice to determine the mechanism and molecular signaling pathway of Ang II regulation of ENaC. We found that Ang II acutely increases ENaC P_o, whereas prolonged exposure to Ang II also induces translocation of α-ENaC toward the apical membrane *in situ*. Ang II actions on ENaC P_o persist in the presence of saturated mineralocorticoid status. Moreover, aldosterone fails to stimulate ENaC acutely, suggesting that Ang II and aldosterone have different time frames of ENaC activation. AT_1 but not AT_2 receptors mediate Ang II actions on ENaC. Unlike its effect in vasculature, Ang II did not increase $[Ca^{2+}]_i$ in split-opened distal nephrons as demonstrated using ratiometric Fura-2-based microscopy. However, application of Ang II to mpkCCD$_{c14}$ cells resulted in generation of reactive oxygen species, as probed with fluorescent methods. Consistently, inhibiting NADPH oxidase with apocynin abolished Ang II-mediated increases in ENaC P_o in murine distal nephron. Therefore, we concluded that Ang II directly regulates ENaC activity in the distal nephron, and this effect complements regulation of ENaC by aldosterone. We propose that stimulation of AT_1 receptors with subsequent activation of NADPH oxidase signaling pathway mediates Ang II actions on ENaC.

Since the seminal work of Guyton (1), it has been recognized that kidneys play central role in controlling circulating volume and consequently blood pressure by regulating the total amount of extracellular sodium via the pressure-natriuresis mechanism. The inability of the kidney to regulate tubular Na^+ reabsorption properly leads to sodium imbalance and blood pressure abnormalities (2). Sodium reabsorption in the aldosterone-sensitive distal nephron (ASDN),[3] which includes the connecting tubule and the cortical collecting duct (CCD), determines final concentration of Na^+ excreted in urine (3–5). Activity of the epithelial Na^+ channel (ENaC) accounts for electrogenic Na^+ reabsorption at this segment (3, 4, 6, 7). Therefore, ENaC is critical for regulation of sodium balance and circulating volume (4, 7–10). The physiological importance of ENaC to regulation of blood pressure in humans is emphasized by inheritable forms of hypertension (Liddle syndrome) resulting from gain-of-function mutations of the channel (5, 9, 11–14). Loss-of-function mutations, in contrast, lead to salt wasting and low blood pressure (pseudohypoaldosteronism type I) (9, 13). ENaC-mediated Na^+ reabsorption also provides the electrical driving force for K^+ secretion mediated by the renal outer medullary K^+ (ROMK) channel and the "big conductance" K^+ channel (15).

ENaC activity in the ASDN is regulated by the renin-angiotensin-aldosterone system (RAAS) in response to variations in dietary Na^+ intake with aldosterone being the primary ENaC activator (4, 6, 7). Elevations in circulating aldosterone levels increase α-ENaC expression and redistribution of β- and γ-ENaC from cytosol to the apical membrane (16, 17). Aldosterone secretion can be stimulated in response to volume depletion (dietary Na^+ restriction) and hyperkalemia (elevated K^+ intake). However, the functional consequences of these eleva-

* This work was supported in part by American Heart Association Grant SDG2230391 (to O. P.), a in part Carl W. Gottschalk research scholar grant from the American Society of Nephrology (to O. P.), National Institutes of Health Grant American Diabetes Association Grant 1-10-BS-168 (to A. S.), and R01HL108880 (to A. S.).
[1] Both authors contributed equally to this work.
[2] To whom correspondence should be addressed: Dept. of Integrative Biology and Pharmacology, University of Texas Health Science Center at Houston, 6431 Fannin, Houston, TX 77030. Tel.: 713-500-7466; Fax: 713-500-7455; E-mail: oleh.m.pochynyuk@uth.tmc.edu.

[3] The abbreviations used are: ASDN, aldosterone-sensitive distal nephron; Ang II, angiotensin II; a.u., arbitrary units; CCD, cortical collecting duct; DOCA, deoxycorticosterone acetate; ENaC, epithelial Na^+ channel; P_o, open probability; PLA_2, phospholipase A_2; PLC, phospholipase C; R, receptor; RAAS, renin-angiotensin-aldosterone system; ROMK, renal outer medullary K^+; ROS, reactive oxygen species; AT_2, angiotensin II receptors type 2; AT_1R, AT_2R, angiotensin II types 1 and 2 receptors.

tions are drastically different, leading to salt retention with little K^+ wasting and kaliuresis with little Na^+ retention, respectively (for review, see Ref. 18), causing the so-called "aldosterone paradox." This leads to the hypothesis that other signaling components of RAAS, such as Ang II, may synergistically contribute to a greater ENaC activation in response to volume contraction. Indeed, correlating evidence suggests that Ang II can stimulate apical Na^+ entry in perfused CCD of rabbits and rats (19). The exact mechanism and signaling pathway of this putative Ang II regulation of ENaC remain obscure. It is also unclear whether this regulation complements antinatriuretic actions of aldosterone on sodium transport in the distal nephron.

The physiological actions of Ang II are mediated by AT_1 and AT_2 receptors (AT_1Rs and AT_2Rs). Activation of AT_1Rs promotes proliferation, vasoconstriction, antinatriuresis, and salt appetite (20). AT_2Rs antagonize many of the biological effects of AT_1Rs by causing vasodilation, apoptosis, and prostaglandin release (21). AT_1 and AT_2 receptors are expressed at both apical and basolateral sides in the ASDN cells, although AT_2R expression is considerably lower (22–24). Stimulation of AT_1Rs can activate a number of downstream signaling cascades, and many of these effects are highly cell-specific. In vasculature smooth muscle cells, AT_1Rs are mainly coupled to $G_{q/11}$-PLC cascade leading to elevations in $[Ca^{2+}]_i$ and muscle contraction (25). In addition, AT_1R stimulation can also activate PI3K, affect arachidonic acid metabolism and promote the formation of reactive oxygen species (ROS) (26). However, little is known about signaling mechanisms that mediate antinatriuretic actions of Ang II in the ASDN.

In this study, we used patch-clamp electrophysiology, immunohistochemistry and ratiometric $[Ca^{2+}]_i$ imaging in freshly isolated split-opened distal nephrons of mice to directly probe regulation of ENaC by Ang II. We found that Ang II increases ENaC activity, and this effect is independent of aldosterone status. Stimulation of AT_1 receptors with subsequent generation of ROS via stimulation of NADPH oxidase mediates Ang II actions on ENaC. Overall, our results provide the first direct support to the idea that the Ang II cascade has its own specific role in stimulating ENaC-mediated sodium reabsorption in response to volume depletion and RAAS activation.

EXPERIMENTAL PROCEDURES

Reagents and Animals—All chemicals and materials were from Sigma, VWR (Radnor, PA), and Tocris (Ellisville, MO) unless noted otherwise and were of reagent grade. Animal use and welfare adhered to the National Institutes of Health Guide for the Care and Use of Laboratory Animals following a protocol reviewed and approved by the Institutional Laboratory Animal Care and Use Committee of the University of Texas Health Science Center at Houston. For experiments, male C57BL/6 mice (purchased from Charles River Laboratories, Wilmington, MA) 6–8 weeks old, were used. Animals were maintained on standard rodent regimen (PURINA 5001) and had free access to tap water. For some experiments, mice were injected with deoxycorticosterone acetate (DOCA) for 3 consecutive days (2.4 mg/injection per animal) prior to the experimentation as we have done previously (29).

Tissue Isolation—The procedure for isolation of the ASDNs containing the connecting tubule and the CCD suitable for electrophysiology and Ca^{2+}-imaging has been described previously (27–29). Briefly, mice were sacrificed by CO_2 administration followed by cervical dislocation; the kidneys were removed immediately. Kidneys were cut into thin slices (<1 mm) with slices placed into ice-cold physiologic saline solution buffered with HEPES (pH 7.4). The ASDN was identified as merging of the connecting tubule into CCD and was mechanically isolated from cortical sections of kidney slices by microdissection using watchmaker forceps under a stereomicroscope. Isolated ASDN was attached to a 5 × 5-mm coverglass coated with poly-L-lysine. A coverglass containing ASDN was placed in a perfusion chamber mounted on an inverted Nikon Eclipse Ti microscope and perfused with room temperature HEPES-buffered (pH 7.4) saline solution. ASDNs were split-opened with two sharpened micropipettes, controlled with different micromanipulators, to gain access to the apical membrane. The tubules were used within 1–2 h of isolation.

Electrophysiology—ENaC activity in principal cells was determined in cell-attached patches on the apical membrane made under voltage clamp conditions ($-V_p = -60$ mV) using standard procedures (28–30). Current recordings were made in a permanently perfused bath (1.5 ml/min). Drug application times are shown with *bars* on the top of representative single channel traces. Recording pipettes had resistances of 8–10 megohms. Typical bath and pipette solutions were: 150 mM NaCl, 5 mM KCl, 1 mM $CaCl_2$, 2 mM $MgCl_2$, 5 mM glucose, and 10 mM HEPES (pH 7.4); and 140 mM LiCl, 2 mM $MgCl_2$ and 10 mM HEPES (pH 7.4), respectively. For each experimental condition, ASDNs from at least three different mice were assayed. Gap-free single-channel current data from gigaohm seals were acquired (and subsequently analyzed) with an Axopatch 200B (Axon Instruments) patch clamp amplifier interfaced via a Digidata 1440 (Axon Instruments) to a PC running the pClamp 10.2 suite of software (Axon Instruments). Currents were low pass-filtered at 100 Hz with an eight-pole Bessel filter (Warner Instruments.). Unitary current was determined, as normal, from all-point amplitude histograms fitted with single- or multi-Gaussian curves using the standard 50% threshold criterion to differentiate between events. Events were inspected visually prior to acceptance. ENaC activity was analyzed over a span of 60–120 s for each experimental condition after reaching a new steady state in response to a treatment. Channel activity, defined as NP_o, was calculated using the following equation: $NP_o = (t_1 + 2t_2 + \ldots + nt_n)$, where N and P_o are the number of ENaC in a patch and the mean open probability of these channels, respectively, and t_n is the fractional open time spent at each of the observed current levels. P_o was calculated by dividing NP_o by the number of active channels within a patch as defined by all-point amplitude histograms. For calculating P_o in paired experiments, N was fixed as the greatest number of active channels observed in control or experimental conditions. To estimate the mean open and closed times of ENaC in ASDN cells carefully from mice kept on standard rodent regimen, we performed dwell time analysis from 56 patch clamp recordings of ENaC activity containing one active channel. The mean open time was 585 ± 58 ms (n = 3,422), and the mean closed time

was 2,775 ± 148 ms ($n = 3,404$). It is known that the number of channels in a patch can be underestimated when P_o is low. To ensure that this was not the case for our experimental conditions, we used an analysis similar to that previously described (31) assuming the estimated open and closed times. From the analysis, we can reliably estimate the maximal number of ENaC in a patch ($p < 0.05$) with observing one visible channel for recording times 1–2 min (90 s average). To further assure reliable calculation of P_o, we measured P_o in patches containing five or fewer channels. Changes in ENaC NP_o in response to a particular treatment in cell-attached experiments most likely reflect changes in P_o because the effects were readily reversible, and we did not observe changes in the number of active states in the majority of recordings. However, the possible changes in ENaC numbers (N) due to trafficking, although improbable, should also be considered.

Immunohistochemistry—Split-opened tubules were fixed with 4% paraformaldehyde in PBS (pH 7.4) for 20 min at room temperature. After fixation, the samples were permeabilized by addition of 0.1% Triton X-100 in PBS for 5 min and washed in PBS three times for 5 min. Nonspecific staining was blocked with 10% normal goat serum (Jackson Immunoresearch) in PBS for 30 min at room temperature. After washing with PBS (three times for 5 min), the samples were incubated for 1.5 h at room temperature in the dark with the primary antibodies against α-ENaC subunit (1:1,000 dilution, generously granted by Mark Knepper's laboratory) dissolved in 1% normal goat serum + 0.1% Triton X-100 in PBS for 3 h at room temperature. Subsequently, samples were incubated for 3 h at room temperature in the dark with goat anti-rabbit IgG labeled with Alexa Fluor 488 (1:400 dilution; Invitrogen) in 1% normal goat serum + 0.1% Triton X-100 in PBS. After washing with PBS (three times for 5 min) the samples were stained with 4′,6-diamidino-2-phenylindole (DAPI) (300 nM concentration; Calbiochem) to visualize nuclei. Subsequently the samples were dehydrated and mounted with permanent mounting medium (Thermo Scientific). Labeled tubules were examined with an inverted Nikon Eclipse Ti fluorescent microscope using a 40× Plan-Fluor oil immersion (1.3 NA) objective. Samples were excited with 488 and 561 nm laser diodes and emission captured with a 16-bit Cool SNAP HQ^2 camera (Photometrics) interfaced to a PC running NIS elements software. Three-dimensional stacks of split-opened ASDNs were generated from series of confocal plane images with 0.25-μm binning step.

$[Ca^{2+}]_i$ Measurements—Intracellular calcium levels were measured in cells of the split-opened ASDNs using Fura-2 fluorescence ratiometric imaging as described previously (32, 33). Split-opened ASDNs were loaded with Fura-2 by incubation with 2 μM Fura-2/AM in a bath solution for 40 min at room temperature. Subsequently, the ASDNs were washed and incubated for an additional 10–15 min prior to experimentation. The ASDNs were then placed in an open top imaging study chamber (Warner RC-10) with a bottom coverslip viewing window and the chamber attached to the microscope stage of an InCa Imaging Work station (Intracellular Imaging). Cells were imaged with a 20× Nikon Super Fluor objective and regions of interest drawn for individual cells. The Fura-2 fluorescence intensity ratio was determined by excitation (an average for ~300 ms) at 340 nm and 380 nm and calculating the ratio of the emission intensities at 511 nm in the usual manner every 5 s. We observed no significant Fura-2 bleaching and minimal Fura-2 leakage at both wavelengths during the experiments. The changes in the ratio were converted to intracellular Ca^{2+} concentrations using the calibration methods as we have done before (34, 35). Experimental traces from individual cells were inspected visually prior to acceptance. Typically, three individual ASDNs from an average of three mice were used for each experimental set.

Cell Culturing—Immortalized mouse cortical collecting duct ($mpkCCD_{c14}$) principal cells were kindly provided by Dr. A. Vandewalle (INSERM, Paris, France) and grown in defined medium on permeable supports (Costar Transwells; 0.4-μm pore, 24-mm diameter) as described previously (36). The cells were maintained with FBS and corticosteroids allowing them to polarize and form a monolayer with high resistance and avid Na^+ reabsorption. The cells were seeded onto permeable supports (Costar Transwells; 0.4-μm pore, 24-mm diameter) at a density of $0.2–0.3 \times 10^6$ cells/filter. The $mpkCCD_{c14}$ cells were kept on filter supports for at least 7 days, and the medium was changed every other day. Growth medium was composed of equal volumes of DMEM and Ham's F12, 60 nM Na^+ selenate, 5 μg/ml transferrin, 50 nM dexamethasone, 1 nM triiodothyronine, 10 ng/ml EGF, 5 μg/ml insulin, 2% FCS, and 100 μg/ml Pen/Strep. The cells were grown in a 5% CO_2/95% air atmosphere incubator at 37 °C. Typically, after 7 days a confluent transporting cell monolayer developed which was subsequently assessed by recording open circuit voltage and trans-epithelial resistance.

Equivalent Open Circuit Current Experiments—A Millicel Electrical Resistance System (Millipore Corp.) was used to measure voltage and resistance across the $mpkCCD_{c14}$ cell monolayers grown on permeable supports (Costar Transwells, 0.4-μm pore, 24-mm diameter), as described previously (36, 37). Equivalent trans-epithelial Na^+ currents were calculated as the quotient of trans-epithelial voltage to trans-epithelial resistance under open-circuit conditions as we reported previously (36).

Total ROS Detection with Fluorescent Microscopy—$MpkCCD_{c14}$ cells were maintained via standard culture practice. The day before the experiment, the cells were seeded onto glass slides to ensure 50–70% confluence on the day of the experiment. The cells were loaded with ROS Detection Solution (Enzo Life Sciences, ENZ-51011) in the DMEM without serum, antibiotics, or supplements according to the manufacturer's protocol and incubated for 1 h. Experimental agents were added to the cells 10 min (vehicle (H_2O) and experimental test agent (Ang II, 1 μM)) or 30 min (ROS inducer (pyocyanin) and negative control reagent (*N*-acetyl-L-cysteine)) prior to the end of the incubation. $MpkCCD_{c14}$ cells loaded with the ROS detection reagent were visualized with fluorescence microscope Eclipse E-600 (Nikon) using a 20× objective equipped with a CCD camera (Princeton Instruments). All images were taken with the same exposure time. The signal was excited at 490 nm, and emission was collected at 525 nm. Fluorescent images were processed with Metamorph 7.5 software (Molecular Devices) and open source software ImageJ 1.42.

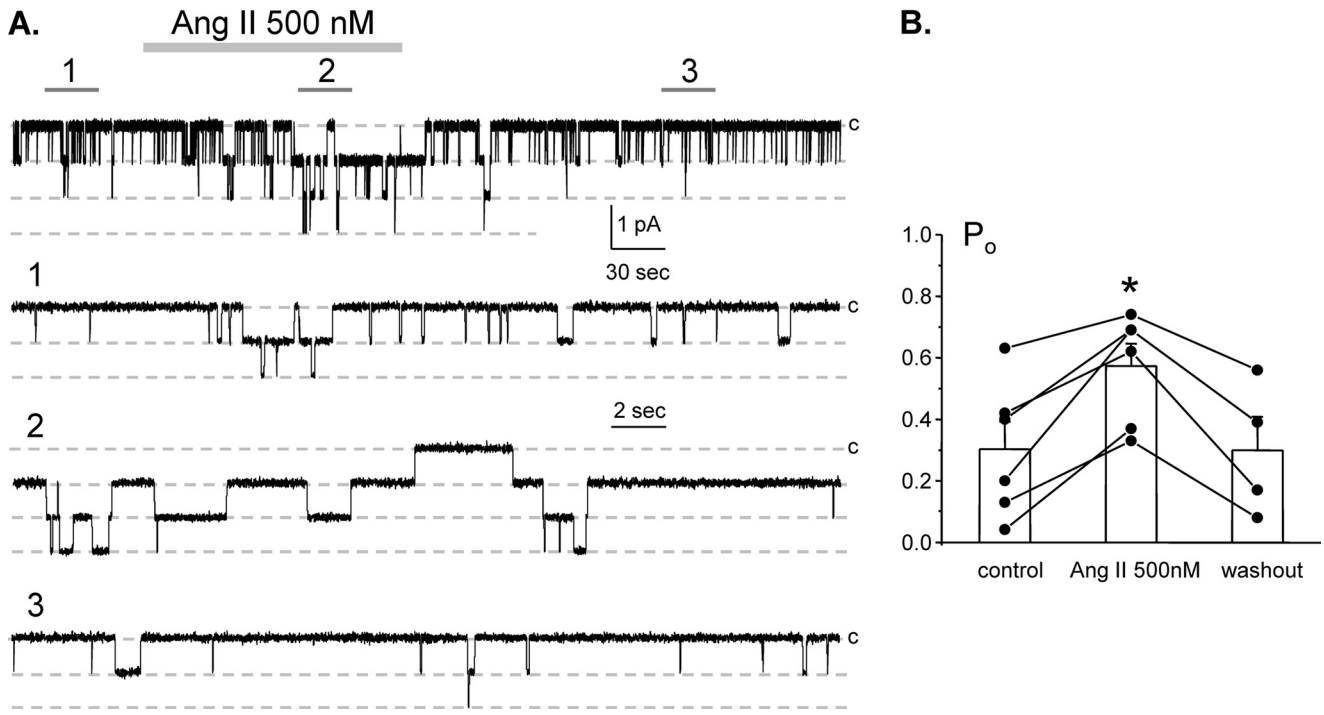

FIGURE 1. **Angiotensin increases ENaC P_o in freshly isolated split-opened ASDNs.** *A*, representative continuous current trace from a cell-attached patch containing at least three ENaCs in the control, under application of 500 nM Ang II, and following washout with regular bath solution. This patch was held at a test potential of $V_h = -V_p = -60$ mV. Areas of control (*1*), upon Ang II treatment (*2*), and washout (*3*) are shown below at an expanded time scale. Inward Li^+ currents are *downward*. *Dashed lines* indicate the respective current state with a *c* denoting the closed state. *B*, summary graph of ENaC P_o changes in response to Ang II and following washing out from paired patch clamp experiments similar to that shown in *A*. *, significant increase *versus* control. *Error bars*, S.E.

Data Analysis—All summarized data are reported as mean ± S.E. Data from before and after treatment within the same experiment were compared using the paired *t* test. Data from different experiments were compared, with a Student's (two-tailed) *t* test or a one-way ANOVA as appropriate. $p < 0.05$ considered significant.

RESULTS

It is well known that elevations of circulating Ang II in response to volume depletion promote aldosterone secretion from zona glomerulosa of the adrenal gland to activate ENaC in the ASDN. Correlative evidence suggests that Ang II might also have more acute effect on Na^+ transport at this nephron segment (19, 38). To test this directly, we used patch clamp electrophysiology in split-opened murine ASDNs to examine Ang II actions on ENaC *in situ*. Fig. 1*A* documents a representative current trace from a cell-attached patch monitoring ENaC activity in the control, during application of 500 nM Ang II and following washout. As can be seen from this paired experiment and the summary graph in Fig. 1*B*, Ang II acutely increases ENaC open probability (P_o) in a reversible manner. The mean P_o was 0.30 ± 0.08, 0.57 ± 0.07, and 0.30 ± 0.10 in the control, during Ang II treatment, and washout, respectively ($n = 6$; $n = 4$ mice).

We next determined the concentration diapason of Ang II regulation of ENaC activity. Fig. 2 summarizes changes in ENaC P_o in paired patch clamp experiments in response to application of different concentrations of Ang II. As is clear, Ang II in concentrations of 20 nM or higher significantly

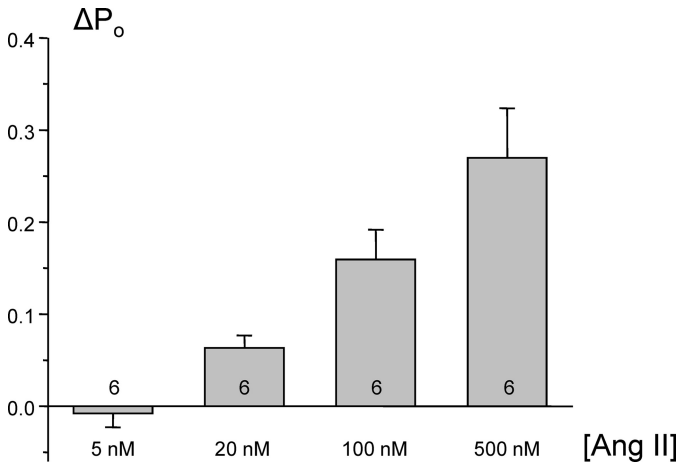

FIGURE 2. **Angiotensin increases ENaC P_o in a dose-dependent manner.** Summary graph of absolute changes in ENaC P_o in response to application of 5, 20, 100, and 500 nM Ang II in paired patch clamp experiments is shown. For each individual experiment the absolute changes were calculated as a difference in ENaC P_o in the control and after application of a respective concentration of Ang II. *Error bars*, S.E.

increased ENaC P_o, whereas 5 nM Ang II had no measurable effect on ENaC.

We next probed whether Ang II and aldosterone are synergistic with regard to stimulation of ENaC in the ASDN. For this, we saturated mineralocorticoid status by injecting mice with DOCA for 3 consecutive days prior to experimentation. Fig. 3*A* contains representative paired experiment monitoring ENaC activity in DOCA-treated animals in the control, during application of Ang II (100 nM), and following washout. As summarized in Fig. 3*B*, the mean P_o was 0.32 ± 0.04, 0.46 ± 0.04, and

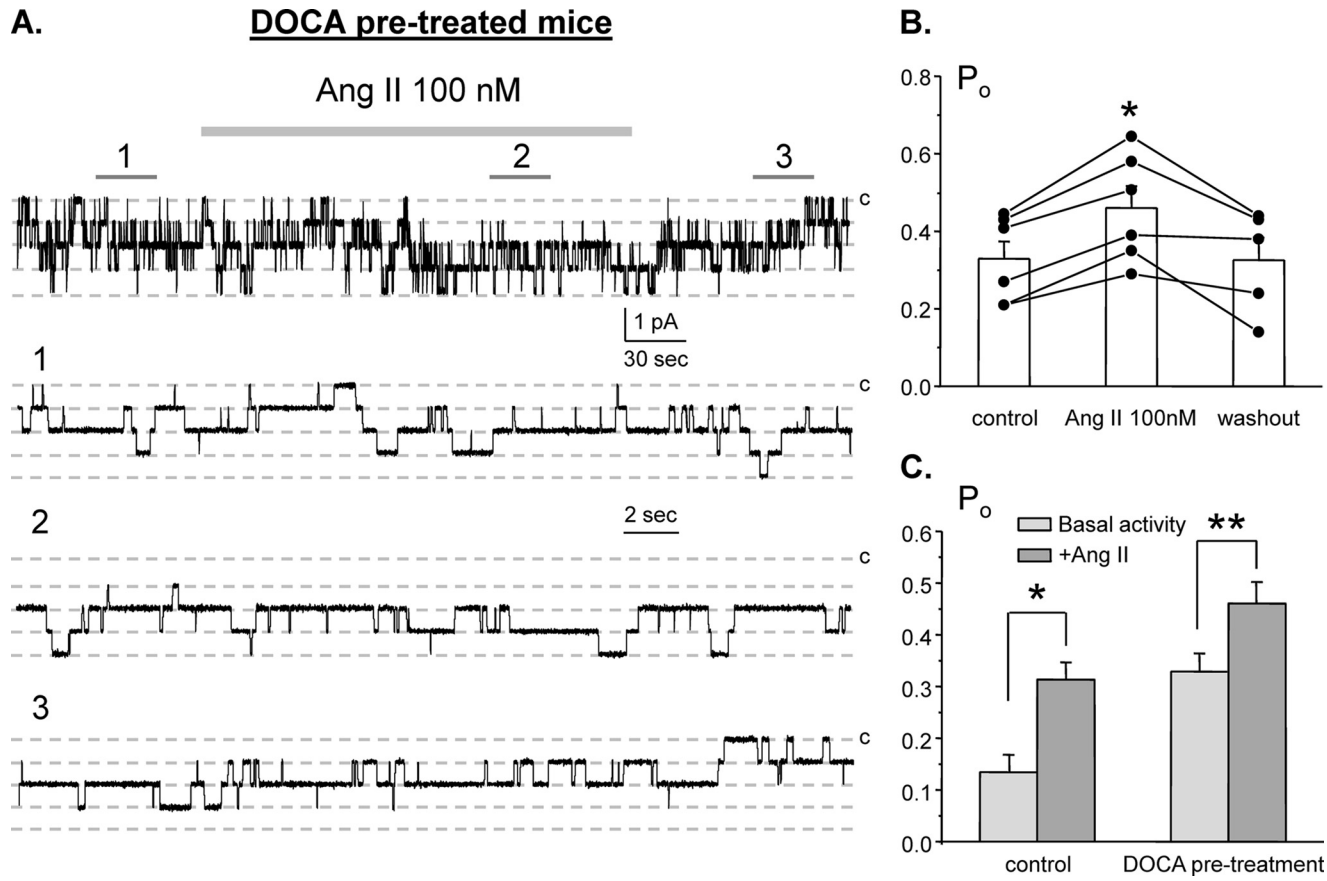

FIGURE 3. **Clamping mineralocorticoids at a high level does not interfere with Ang II actions on ENaC.** *A*, representative continuous current trace from a cell-attached patch monitoring ENaC activity in the control, under application of 100 nM Ang II, and following washout with regular bath solution. For these experiments animals were injected with DOCA for 3 consecutive days prior to the experimentation. Areas of control (*1*), after Ang II treatment (*2*), and washout (*3*) are shown below at an expanded time scale. All other conditions are identical to those described in Fig. 1*A*. *B*, summary graph of ENaC P_o changes in response to 100 nM Ang II and following washing out from paired patch clamp experiments similar to that shown on *A*. *, significant increase *versus* control. *C*, summary graph comparing actions of 100 nM Ang on average ENaC P_o in control and in DOCA-treated mice. *, significant increase *versus* control basal activity; **, significant increase *versus* DOCA pretreatment basal activity. *Error bars*, S.E.

0.32 ± 0.05 in the control, following application of Ang II, and washout, respectively ($n = 6$, $n = 5$ mice). The comparison of Ang II effects in the control and in DOCA-treated mice is shown in Fig. 3*C*. As is clear from the results in Fig. 3, the effect of Ang II on ENaC is preserved when mineralocorticoid levels are clamped high.

To probe further whether Ang II and aldosterone have distinct stimulatory actions on ENaC, we determine the acute effects of aldosterone on ENaC P_o. Fig. 4*A* demonstrates a representative experiment monitoring changes in ENaC activity in cell-attached configuration in the control, during application of 10 nM aldosterone (5 min) and following washout. As can be seen from this representative experiment and the summary graph in Fig. 4*B*, aldosterone failed to stimulate ENaC acutely in these native preparations. The mean P_o was 0.23 ± 0.08 and 0.21 ± 0.08 in the control and following aldosterone application, respectively ($n = 7$, $n = 3$ mice). This contrasts with the acute activation of ENaC by Ang II (Figs. 1–3), suggesting that aldosterone and Ang II have different time frames of ENaC stimulation and, thus, distinct mechanisms of actions.

We next tested the signaling determinants of Ang II regulation of ENaC in the distal nephron. Fig. 5*A* shows a representative current trace containing a single ENaC in the control, during inhibition of AT_1R with losartan (1 μM), and following application of Ang II (500 nM) in the continued presence of the antagonist. As summarized in Fig. 5*B*, Ang II fails to increase ENaC activity when AT_1Rs are inhibited.

We further tested whether AT_2R has a complementary role in regulation of ENaC by Ang II. Fig. 5*C* shows a continuous patch clamp experiment monitoring ENaC activity in the control, after direct stimulation of AT_2R with a selective agonist, CGP42112 (100 nM), and following washout. As summarized in Fig. 4*D*, stimulation of AT_2Rs has little effect on ENaC P_o. The mean P_o was 0.29 ± 0.06 and 0.25 ± 0.06 in the control and following CGP42112 application, respectively ($n = 10$, $n = 7$ mice). Overall, we concluded that Ang II increases ENaC activity by stimulating AT_1 but not AT_2 receptors.

AT_1Rs are typically coupled to $G_{q/11}$ in vasculature cells leading to stimulation of PLC and elevations of $[Ca^{2+}]_i$ via an IP_3-sensitive mechanism (25). To test whether stimulation of AT_1Rs initiates similar signaling cascade in ASDN, we directly monitored changes in $[Ca^{2+}]_i$ in individual cells within a split-opened area using Ca^{2+}-sensitive dye Fura-2. As a positive control, we stimulated purinergic cascade with ATP to elevate $[Ca^{2+}]_i$ in ASDN cells as we reported previously (35, 39). Appli-

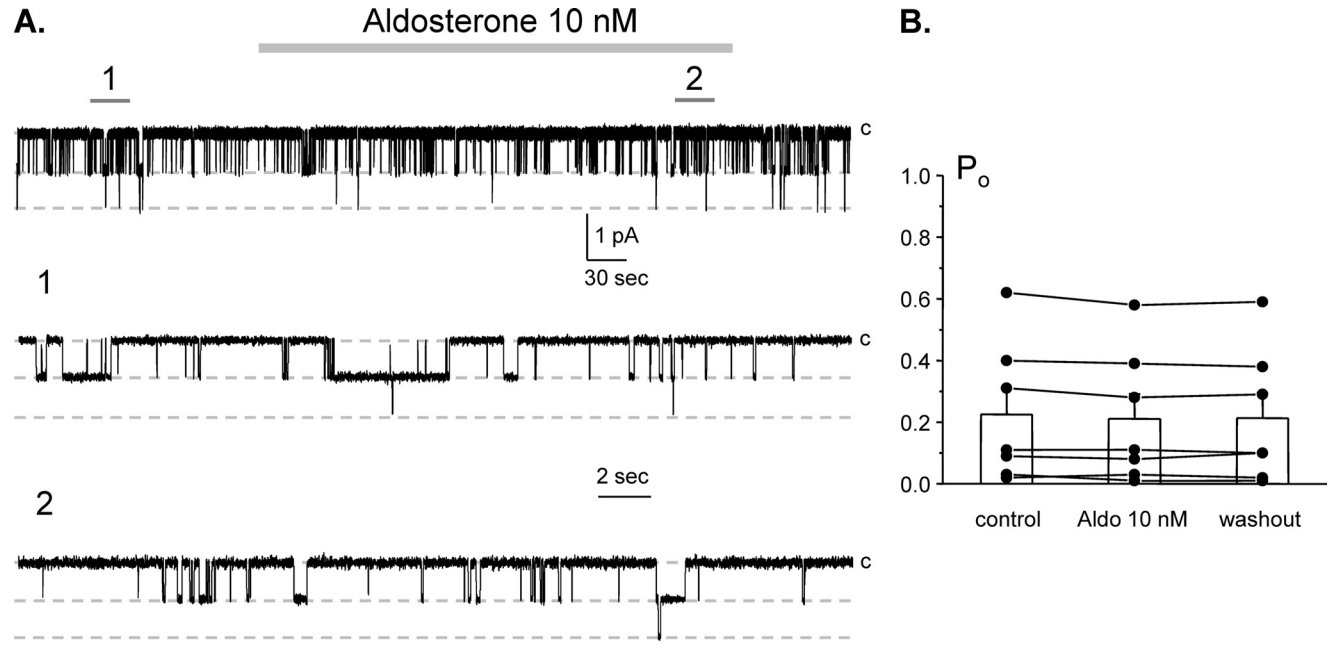

FIGURE 4. **Aldosterone does not acutely affect ENaC P_o in freshly isolated split-opened ASDNs.** *A*, representative continuous current trace from a cell-attached patch containing two ENaCs in the control, under application of 10 nM aldosterone, and following washout with regular bath solution. Areas of control (*1*) and after aldosterone (*2*) are shown below at an expanded time scale. All other conditions are identical to those described in Fig. 1*A*. *B*, summary graph of ENaC P_o changes in response to 10 nM aldosterone from paired patch clamp experiments similar to that shown in *A*. *Error bars*, S.E.

cation of 10 μM ATP produces a transient peak followed by a sustained plateau (Fig. 6*A*). In contrast, subsequent application of 500 nM Ang II fails to induce measurable $[Ca^{2+}]_i$ elevations. To exclude a possibility that Ang II-mediated Ca^{2+} changes might be compromised by the prior exposure to ATP, we reversed the order of agonist applications. Consistently, Ang II failed to increase $[Ca^{2+}]_i$ whereas subsequent purinergic stimulation induced prominent elevation of $[Ca^{2+}]_i$ (Fig. 6*B*). We concluded that Ang II does not activate PLC-IP_3-$[Ca^{2+}]_i$ cascade in ASDN cells.

AT_1R-mediated signal transduction cascades can also involve activation of PI3K and PLA_2 (26). To determine whether Ang II increases ENaC P_o via a PI3K-sensitive mechanism, we treated split-opened ASDN with a selective PI3K inhibitor, LY294002 (20 μM). LY294002 application significantly decreased ENaC P_o from 0.52 $\pm$ 0.06 to 0.14 $\pm$ 0.03 ($n = 8$, $n = 4$ mice). However, Ang II was capable of increasing ENaC P_o to 0.32 $\pm$ 0.05 in the continued presence of the inhibitor (Fig. 7*A*). We concluded that PI3K plays a minor role in signaling pathway of ENaC regulation by Ang II.

We next tested whether Ang II increases ENaC P_o in a PLA_2-dependent manner. Inhibition of PLA_2 with a selective inhibitor, AACOCF3 (30 μM), decreases ENaC P_o from 0.41 $\pm$ 0.04 to 0.20 $\pm$ 0.04 ($n = 13$, $n = 6$ mice). Ang II significantly increased ENaC P_o to 0.38 $\pm$ 0.05 on the background of the PLA_2 inhibitor (Fig. 7*B*). These results exclude PLA_2 as having a role in signaling pathway coupling Ang II actions to changes in ENaC activity.

Ang II is known to increase production of ROS via activation of NADPH oxidase complex in many cell types (26). Therefore, we next probed whether activation of NADPH oxidase mediates Ang II actions on ENaC. Fig. 8*A* contains a representative patch clamp experiment monitoring ENaC activity in the control, after application of apocynin (100 μM), application of 500 nM Ang II in the continued presence of the former, and following washout. Apocynin, which blocks NADPH oxidase subunit assembly (40), does not affect ENaC activity by itself. However, treatment with apocynin abolished stimulatory action of Ang II on ENaC. The mean P_o was 0.37 $\pm$ 0.04, 0.31 $\pm$ 0.05, and 0.22 $\pm$ 0.06 ($n = 9$, $n = 5$ mice) in the control, during apocynin application, and following Ang II in the continued presence of the inhibitor, respectively (Fig. 8*B*). These results are consistent with Ang II stimulating ENaC P_o in a NADPH oxidase-dependent manner.

To test further whether Ang II increases ENaC activity by promoting ROS production, we next directly assessed total ROS levels in cultured $mpkCCD_{c14}$ cells in response to Ang II. Fig. 9*A* demonstrates representative micrographs of the fluorescent ROS reporter after 10 min treatment with vehicle (*left*) and 1 μM Ang II (*right*). The negative and positive controls (*N*-acetyl-L-cysteine and pyocyanin, respectively) are shown below. As documented by the summary graph in Fig. 9*B*, Ang II treatment significantly increased fluorescence levels to 1,463.07 $\pm$ 52.26 a.u. compared with 718.03 $\pm$ 39.05 a.u. in the control. The negative and positive controls have fluorescent values of 19.50 $\pm$ 5.08 a.u. and 1,977.00 $\pm$ 19.18 a.u., respectively.

To verify that Ang II stimulates ENaC-mediated sodium transport in $mpkCCD_{c14}$ cells as it occurs in freshly isolated ASDNs, we have studied the effects of Ang II on equivalent I_{oc}. As shown in Fig. 9*C*, application of 1 μM Ang II to polarized $mpkCCD_{c14}$ cells significantly increased amiloride-sensitive open circuit current in a time-dependent manner. These data demonstrate that the time course of ROS generation in response to Ang II parallels with stimulation of sodium transport in cultured principal cells.

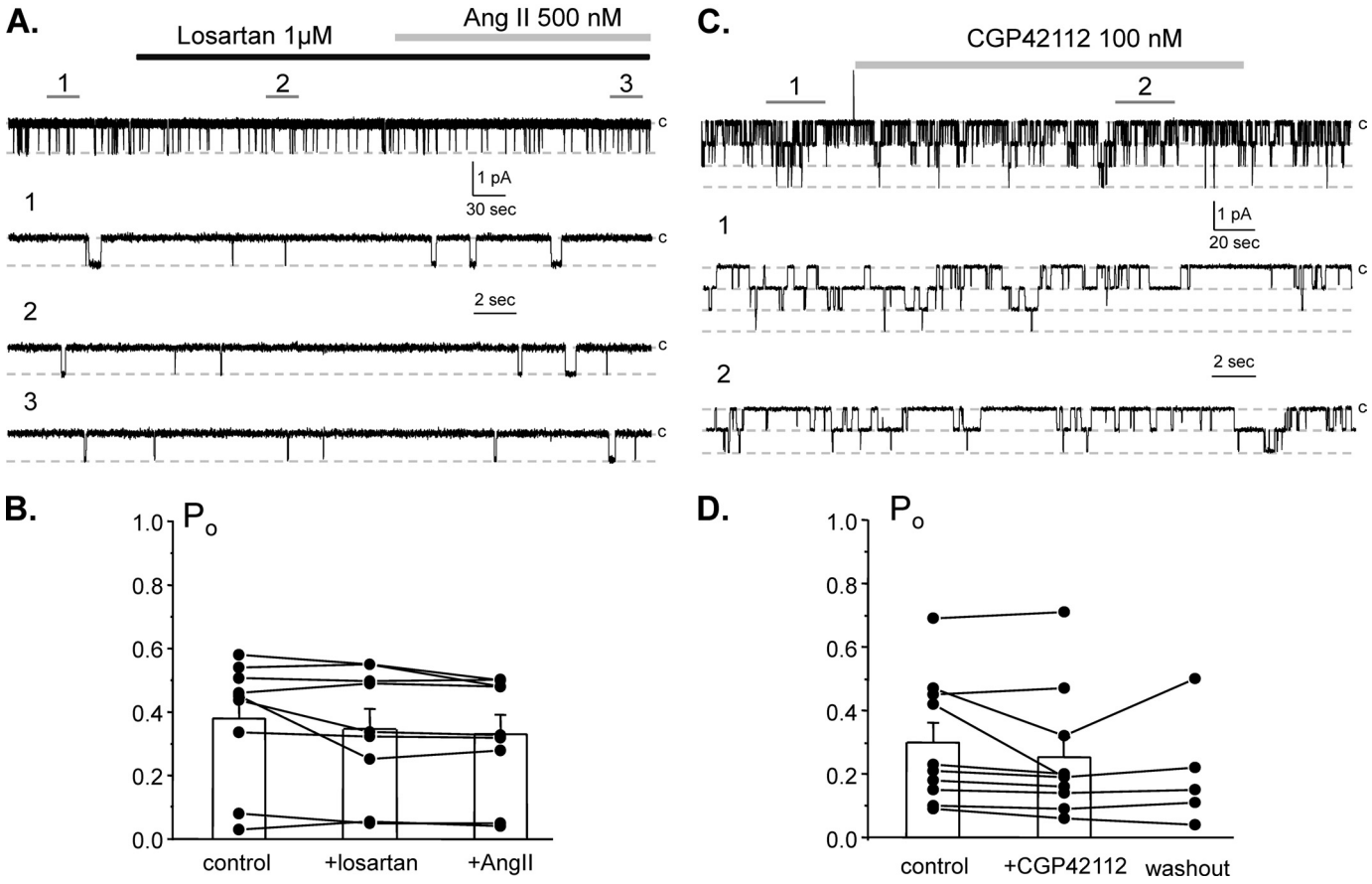

FIGURE 5. **Ang II increases ENaC activity by stimulating AT_1 receptors.** *A*, representative continuous current trace from a cell-attached patch containing a single ENaC in the control, after inhibition of AT_1 receptors with a selective antagonist, 1 μM losartan, and following application of 500 nM Ang II in the continued presence of the AT_1R antagonist. Areas of control (*1*), after losartan (*2*), and following Ang II (*3*) are shown below with an expanded scale. *B*, summary graph of ENaC P_o changes in response to the AT_1R antagonist and following Ang II treatment from paired patch clamp experiments similar to those shown in *A*. *C*, representative continuous current trace from a cell-attached patch monitoring ENaC activity in the control, after stimulation of AT_2 receptors with a selective agonist, 100 nM CGP42112, and following washout with control solution. Areas of control (*1*) and after CGP42112 (*2*) are shown below with an expanded time scale. *D*, summary graph of ENaC P_o changes in response to the AT_2R agonist and following washout from paired patch clamp experiments similar to shown in *C*. *Error bars*, S.E.

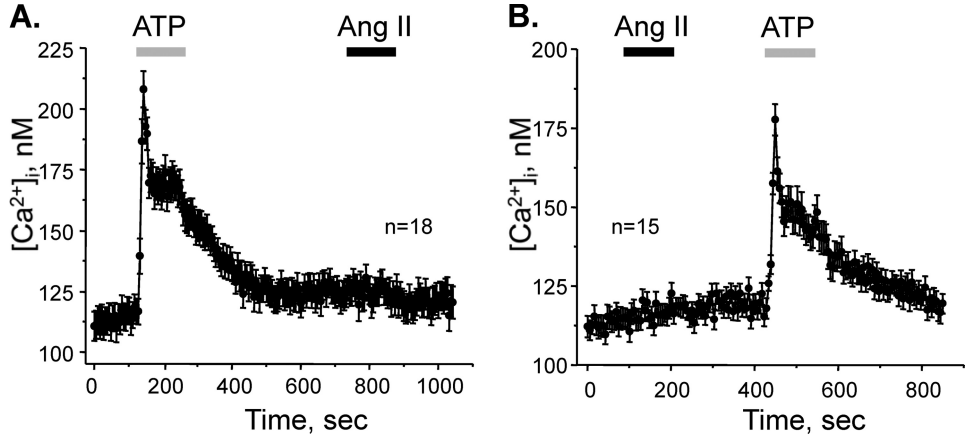

FIGURE 6. **Ang II does not increase $[Ca^{2+}]_i$ in ASDN cells.** *A*, average time course of $[Ca^{2+}]_i$ changes in individual cells of ASDN in response to 2-min application of 10 μM ATP (shown with a *gray bar*) and 500 nM Ang II (shown with a *black bar*). *B*, average time course of $[Ca^{2+}]_i$ changes in individual cells of distal nephron in response to 2-min application of 500 nM Ang II (shown with a *black bar*) and 10 μM ATP (shown with a *gray bar*).

We finally probed whether prolonged exposure to Ang II may also affect membrane ENaC levels. For this, we pretreated split-opened ASDNs with either vehicle or Ang II for 30 min. Fig. 10*A* shows representative current traces of ENaC activity after treatment with vehicle (*top*) and 500 nM Ang II (*bottom*). For quantification of Ang II actions on ENaC, we estimated integral ENaC activity (fNP_o), where N is the number of active channels per patch and f is the frequency of observing patches with at least one active channel (f = number of patches with channels/total number of patches). As summarized in Fig. 10*B*,

Ang II significantly increases fNP_o from 0.32 ± 0.04 (n = 102 patches) to 0.80 ± 0.10 (n = 45 patches). This was associated with an increased P_o from 0.36 ± 0.03 (n = 48 patches with channels) to 0.51 ± 0.03 (n = 25 patches with channels). Importantly, we have also observed a significant increase in N from 1.81 ± 0.18 to 3.0 ± 0.3.

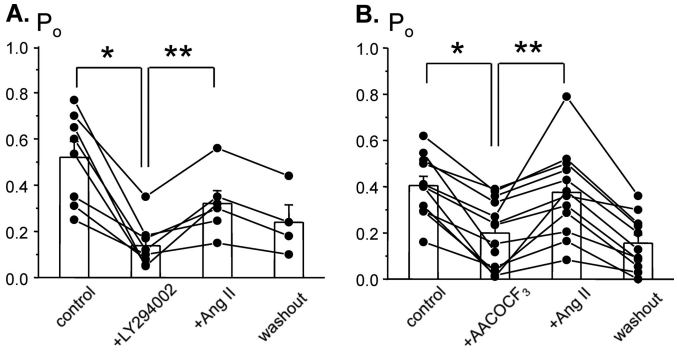

FIGURE 7. **Ang II regulation of ENaC does not involve PI3K and PLA_2.** *A*, summary graph of ENaC open probability changes in response to inhibition of PI3K with LY294002 (20 μM), application of 500 nM Ang II in the continued presence of the antagonist, and following washout with control solution from paired patch clamp experiments performed on isolated split-opened ASDNs. *, significant decrease *versus* control; **, significant increase *versus* +LY294002. *B*, summary graph of ENaC P_o changes in response to inhibition of PLA_2 with $AACOCF_3$ (30 μM), application of 500 nM Ang II in the continued presence of the antagonist, and following washout with control solution from paired patch clamp experiments performed on isolated split-opened ASDNs. *, significant decrease *versus* control; **, significant increase *versus* + $AACOCF_3$. *Error bars*, S.E.

The effect of Ang II on the functional ENaC levels can result from facilitated ENaC trafficking and/or activation of the silent channels on the apical membrane. To test this further, we next directly visualized ENaC redistribution in split-opened ASDNs in response to Ang II with immunohistochemistry. Fig. 11*A* demonstrates representative fluorescent confocal images of αENaC localization within principal cells treated with vehicle (*left*) and 500 nM Ang II (*middle*) for 30 min. α-ENaC has diffuse distribution on the apical side of principal cells during control conditions. Importantly, Ang II treatment caused a prominent shift of the fluorescent signal toward the apical membrane. As a positive control, we treated split-opened ASDNs with 10 μM forskolin which was reported to promote ENaC trafficking in cultured distal nephron cells via activation of protein kinase A and elevation of cAMP levels (41). For quantitative estimation, we employed line scan analysis of α-ENaC distribution along z axis in cross-sections of three-dimensional stacks similar to that shown in Fig. 11*A*. The graph in Fig. 11*B* shows dependence of the relative fluorescent intensity from the position on the z axis in individual cells of ASDN treated with vehicle, Ang II, and forskolin, respectively. As is clear, Ang II and forskolin caused a leftward narrowing of the bell-shape distribution of α-ENaC along z axis. As summarized in Fig. 11*C*, the half-width was significantly reduced from 1.58 ± 0.03 μm in the control to 1.07 ± 0.02 μm and 0.86 ± 0.03 μm in response to Ang II and forskolin, respectively. The results in

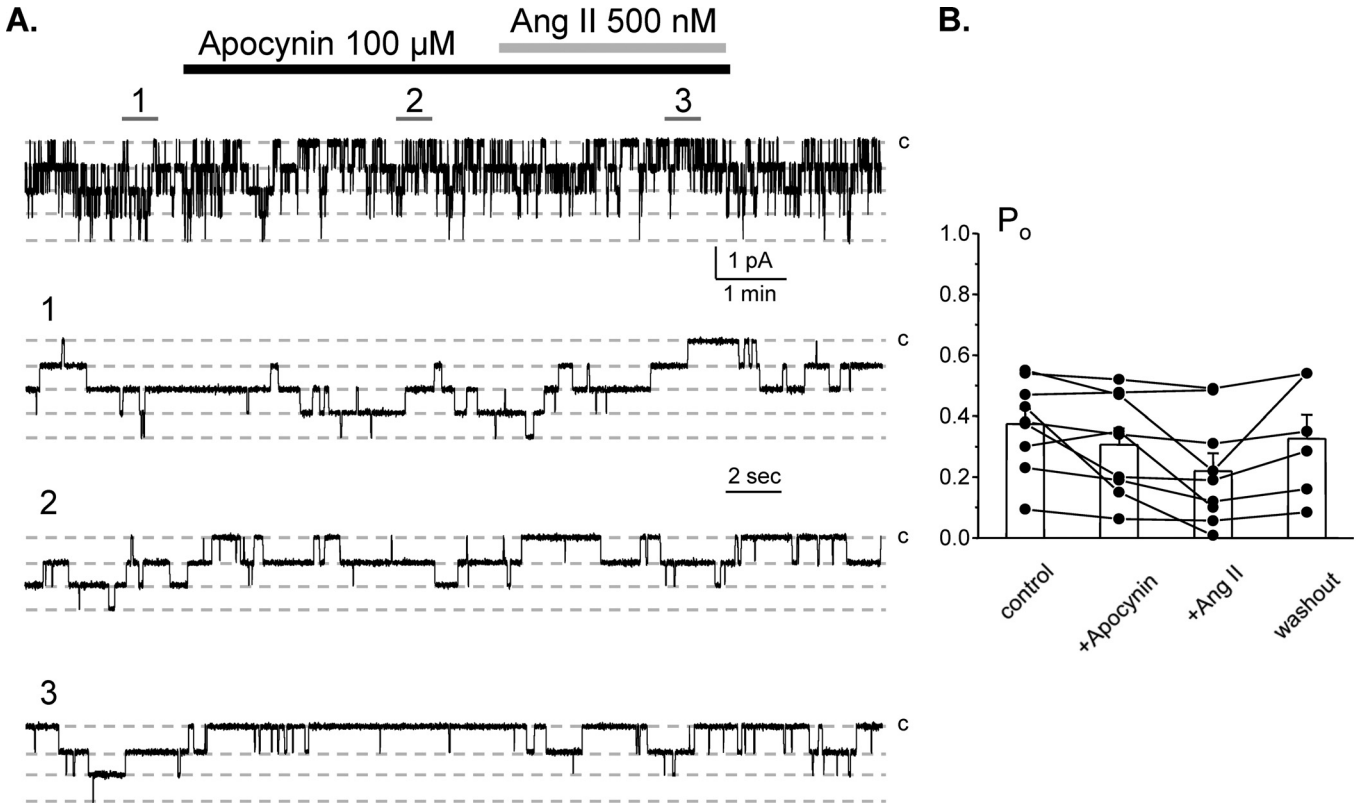

FIGURE 8. **Stimulatory effect of Ang II on ENaC is mediated by NADPH oxidase.** *A*, representative continuous current trace from a cell-attached patch containing monitoring ENaC activity in the control, after inhibition of NADPH oxidase with 100 μM apocynin, application of 500 nM Ang II in the continued presence of the former, and following washout with control solution. Areas of control (*1*), after apocynin (*2*), and following Ang II (*3*) are shown below with an expanded scale. *B*, summary graph of ENaC P_o changes in response to the inhibition of NADPH oxidase, Ang II treatment, and washout from paired patch clamp experiments similar to those shown in *A*. *Error bars*, S.E.

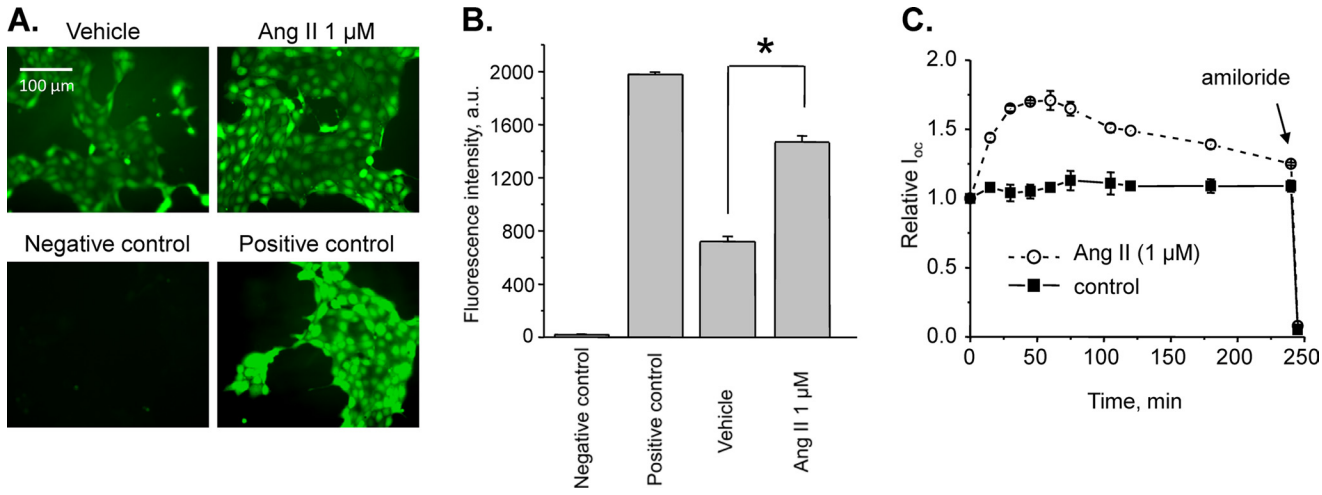

FIGURE 9. **Ang II induces formation of ROS and stimulates amiloride-sensitive I_{oc} in mpkCCD$_{c14}$ cells.** *A*, representative fluorescent micrographs of the mpkCCD$_{c14}$ cells loaded with the total ROS detection reagent treated with a vehicle (control), 1 μM Ang II, ROS inhibitor (*N*-acetyl-L-cysteine, negative control), and ROS inducer (pyocyanin, positive control). *Scale bar* shown is common for all images. *B*, summary graph of ROS detection experiments ($n = 25$) displaying the total fluorescence intensity measured from the images of the mpkCCD$_{c14}$ cells treated with different experimental agents. Background fluorescence level was corrected. *, significant increase *versus* vehicle. *C*, summary graph of equivalent I_{oc} in mpkCCD$_{c14}$ principal cells in response to 1 μM Ang II. Ang II and vehicle (control) were added at time 0, and the current was normalized to the starting level. Amiloride (10 μM; *arrow*) was added to the apical membrane at the end of experiments. Values are means ± S.E. (*error bars*) of at least three experiments for each value.

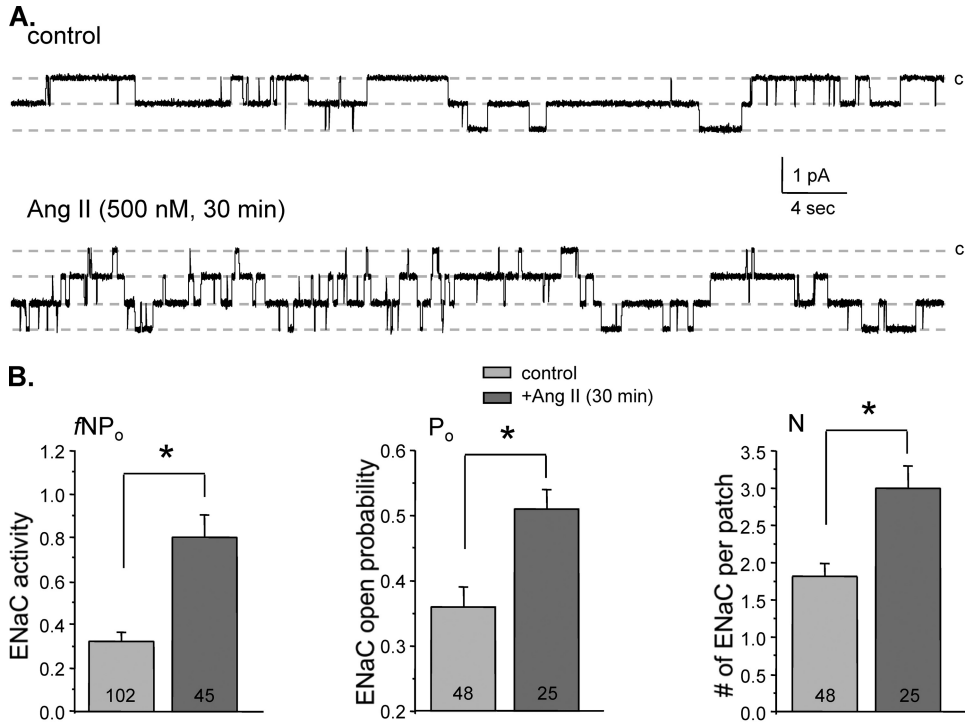

FIGURE 10. **Prolonged Ang II treatment stimulates ENaC in the ASDNs by increasing both open probability and functional ENaC numbers.** *A*, representative current traces of ENaC activity in the control (*top*) and after application of 500 nM Ang II for 30 min (*bottom*). All other conditions are identical to those described in Fig. 1*A*. *B*, summary graphs comparing integral ENaC activity (fNP_o, *left*), ENaC open probability (P_o, *middle*), and number of active channels per patch (*N*, *right*) for split-opened ASDNs treated with vehicle and Ang II for 30 min. *, significant increase *versus* control. *Error bars*, S.E.

Fig. 11 suggest that prolonged exposure of ASDNs to Ang II induces prominent redistribution of α-ENaC from cytosol compartments toward the apical membrane. This is the first demonstration of direct effect of Ang II on ENaC trafficking *in situ* that we are aware of.

DISCUSSION

The classical model of sodium transport regulation in the distal nephron postulates that variations in systemic salt intake control ENaC-mediated sodium reabsorption via aldosterone-mediated mechanisms. In this study, we expand this view by providing experimental evidence that Ang II, in addition to its well known stimulatory actions on aldosterone secretion from the adrenal gland, has a direct effect on ENaC activity in native murine distal nephron. This regulation is complex and includes an acute activation of functional ENaC as well as more chronic effect on ENaC trafficking to the apical plasma membrane (Fig. 12).

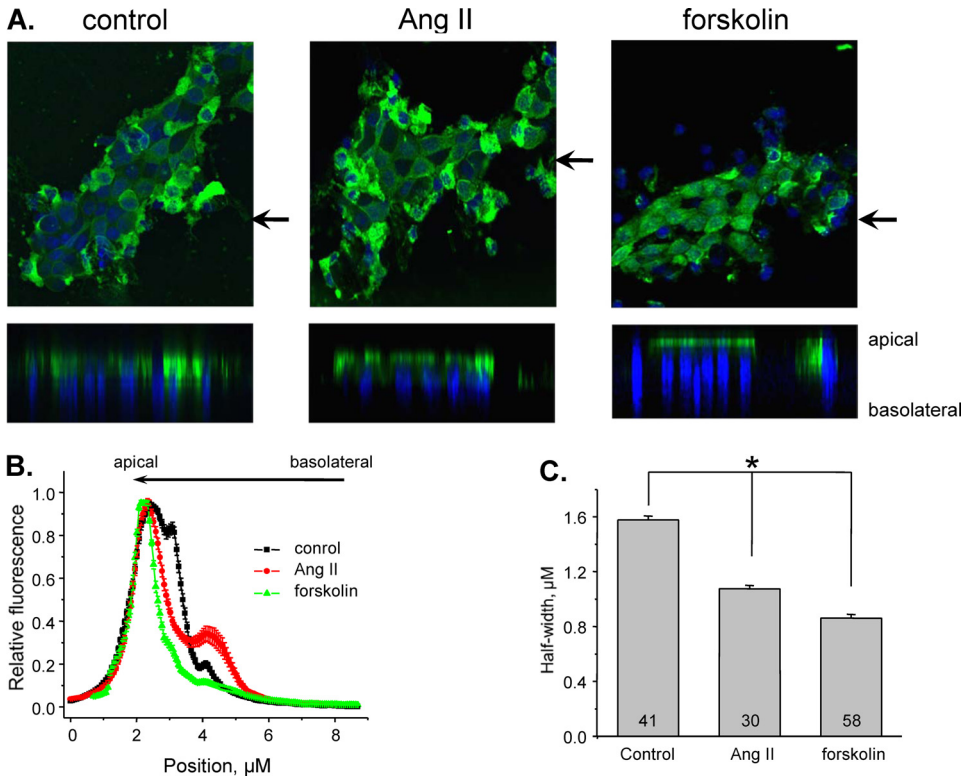

FIGURE 11. **Ang II induces translocation of α-ENaC toward the apical membrane.** *A*, representative confocal plane images (*top*) and corresponding cross-sections of three-dimensional stacks by *z* axis (*bottom*) of α-ENaC localization (pseudocolor *green*) in split-opened ASDNs treated for 30 min with vehicle (*left*), 500 nM Ang II (*middle*), and 10 μM forskolin (*right*). Nuclear DAPI staining is also shown (pseudocolor *blue*). The positions of cross-section are shown by the *arrows*. *B*, distribution of averaged relative fluorescent signals representing α-ENaC localization along a line on *z* axis crossing a cell upon treatment with vehicle, Ang II, and forskolin. For each individual cell the fluorescent signals were normalized to their corresponding maximal value. The positions of the apical and basolateral sides are shown with *arrows* at the *top*. *C*, summary graph of half-width means for distributions of fluorescent signals shown in *B*. *, significant decrease *versus* control. *Error bars*, S.E.

It has been found previously that application of Ang II stimulates luminal Na^+ entry in the perfused CCD of rabbits (19). Using patch clamp electrophysiology in freshly isolated split-opened murine distal nephrons, we determined directly that nanomolar concentrations of Ang II acutely increase ENaC P_o. Physiological concentrations of Ang II in the ASDN have as yet to be carefully estimated. However, Ang II concentration in the fluid sampled from the proximal tubule greatly exceeds 10^{-8} M (42). Moreover, an existence of intrarenal RAS in the distal nephron allows local generation of Ang II *in situ* (for review, see Ref. 43). Indeed, application of Ang I stimulates apical Na^+ entry in perfused CCDs in an angiotensin-converting enzyme-dependent manner (44), suggesting that the rate of paracrine conversion of Ang I to Ang II is sufficient to activate Ang II receptors. Furthermore, the Ang II concentrations can be markedly elevated during pathophysiological conditions (45).

We determined that activation of AT_1R is necessary for Ang II-mediated regulation of ENaC P_o. This is in a good agreement with observation that inhibition of AT_1R abolishes Ang II-mediated luminal Na^+ entry in the perfused CCDs (19). Interestingly, we found that Ang II had little effect on $[Ca^{2+}]_i$ in ASDN cells, suggesting that AT_1R do not activate $G_{q/11}$-PLC pathway as it commonly occurs in vasculature cells (26, 46). This makes sense as activation of this signaling cascade leads to inhibition of ENaC in the ASDN via purinergic and bradykinin signaling cascades as we have reported previously (28, 39).

Ang II induces generation of ROS in many tissues including vascular smooth muscle cells, endothelial cells, phagocytic cells, and fibroblasts (26), resulting chiefly from activation of NADPH oxidases. Moreover, it was recently demonstrated that Ang II inhibits activity of ROMK-like channels in the CCD in a NADPH oxidase-dependent manner (47). In our study, we also identified a critical role of NADPH oxidase in signaling pathway of Ang II regulation of ENaC. A common signaling mechanism of Ang II regulation of sodium and potassium transport supports an idea that Ang II via stimulation of NADPH oxidases plays an important role in uncoupling sodium reabsorption by stimulating ENaC from potassium secretion by inhibiting ROMK in ASDN. Indeed, a recent study demonstrates that Ang II inhibits activity of ROMK1 during condition of volume depletion (48). Furthermore, we directly demonstrated that Ang II increases ROS production in cultured mouse principal cells. A recent report suggests that ROS, specifically H_2O_2, possess a stimulatory effect on ENaC P_o in A6 cells (49). This effect was not direct and involved activation of PI3K. In contrast, we found a minor role of PI3K in Ang II regulation of ENaC in native murine ASDN. We predict that different species may cause this apparent discrepancy. Thus,

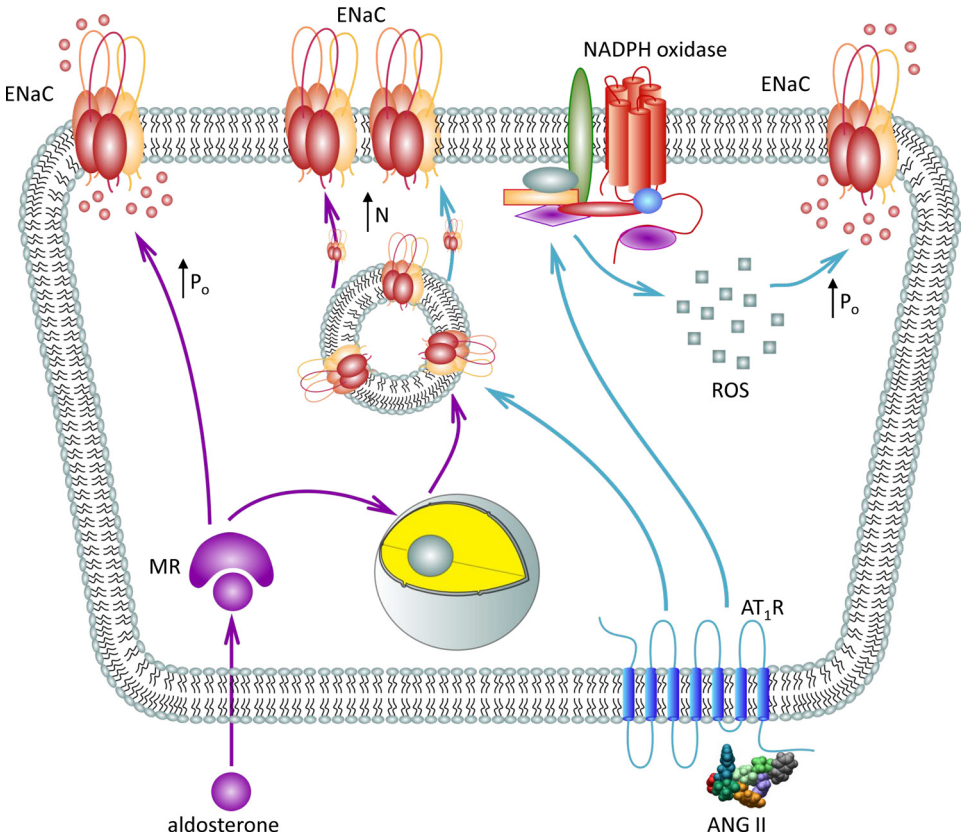

FIGURE 12. **Principal scheme of ENaC regulation by Ang II in the ASDN.**

subunit composition of NADPH complex and expression of cell-specific NADPH oxidase isoforms can be critical for Ang II regulation of ENaC. Therefore, the exact mechanism of ENaC regulation by ROS in mammalian ASDN requires further examination.

In this study, we provide the first direct evidence that Ang II, in addition to stimulation of ENaC P_o, increases ENaC abundance on the apical plasma membrane. Indeed, prolonged Ang II treatment increases the number of functional channels within a patch. Moreover, we observed translocation of α-ENaC from cytosol toward the plasma membrane in response to Ang II treatment in split-opened murine distal nephrons. This regulation is physiologically relevant because mice lacking AT_1Rs exhibit a marked reduction in α-ENaC abundance despite slightly elevated aldosterone levels (50). Similarly, systemic AT_1R blockade also decreases α-ENaC protein levels, and this effect is not prevented by inhibition of mineralocorticoid receptors with spironolactone (51).

Overall, this paper provides direct evidence that Ang II possesses multiple stimulatory actions on ENaC and that its effect is preserved in the presence of saturated systemic mineralocorticoids. Moreover, we demonstrate that the effects of Ang II and aldosterone have different time courses of ENaC activation. The synergy between aldosterone and Ang II may play an important physiological role in maximizing ENaC-mediated sodium reabsorption in the ASDN under conditions of volume depletion to minimize sodium loss with urine. Conversely, aldosterone-independent regulation of ENaC by Ang II might have detrimental consequences on sodium balance under pathological conditions that cause overstimulation of the intrarenal RAS, such as diabetes mellitus (for review, see Ref. 45), leading to hypertension and kidney damage.

REFERENCES

1. Guyton, A. C. (1991) *Science* **252,** 1813–1816
2. Khawaja, Z., and Wilcox, C. S. (2011) *Int. J. Hypertens.* **2011,** 143471
3. Garty, H., and Palmer, L. G. (1997) *Physiol. Rev.* **77,** 359–396
4. Hummler, E. (2003) *Curr. Hypertens. Rep.* **5,** 11–18
5. Lifton, R. P., Gharavi, A. G., and Geller, D. S. (2001) *Cell* **104,** 545–556
6. Eaton, D. C., Malik, B., Saxena, N. C., Al-Khalili, O. K., and Yue, G. (2001) *J. Membr. Biol.* **184,** 313–319
7. Schild, L., and Kellenberger, S. (2001) *Adv. Exp. Med. Biol.* **502,** 305–314
8. Hummler, E. (1999) *J. Steroid Biochem. Mol. Biol.* **69,** 385–390
9. Schild, L. (2004) *Rev. Physiol. Biochem. Pharmacol.* **151,** 93–107
10. Stockand, J. D. (2002) *Am. J. Physiol. Renal Physiol.* **282,** F559–576
11. Hansson, J. H., Schild, L., Lu, Y., Wilson, T. A., Gautschi, I., Shimkets, R., Nelson-Williams, C., Rossier, B. C., and Lifton, R. P. (1995) *Proc. Natl. Acad. Sci. U.S.A.* **92,** 11495–11499
12. Hansson, J. H., Nelson-Williams, C., Suzuki, H., Schild, L., Shimkets, R., Lu, Y., Canessa, C., Iwasaki, T., Rossier, B., and Lifton, R. P. (1995) *Nat. Genet.* **11,** 76–82
13. Schild, L. (1996) *Nephrologie* **17,** 395–400
14. Shimkets, R. A., Warnock, D. G., Bositis, C. M., Nelson-Williams, C., Hansson, J. H., Schambelan, M., Gill, J. R., Jr., Ulick, S., Milora, R. V., and Findling, J. W. (1994) *Cell* **79,** 407–414
15. Wang, W. H., and Giebisch, G. (2009) *Pflugers Arch.* **458,** 157–168
16. Knepper, M. A., Kim, G. H., and Masilamani, S. (2003) *Ann. N.Y. Acad. Sci.* **986,** 562–569
17. Masilamani, S., Kim, G. H., Mitchell, C., Wade, J. B., and Knepper, M. A. (1999) *J. Clin. Invest.* **104,** R19–23
18. Arroyo, J. P., Ronzaud, C., Lagnaz, D., Staub, O., and Gamba, G. (2011) *Physiology* **26,** 115–123

19. Peti-Peterdi, J., Warnock, D. G., and Bell, P. D. (2002) *J. Am. Soc. Nephrol.* **13,** 1131–1135
20. Berry, C., Touyz, R., Dominiczak, A. F., Webb, R. C., and Johns, D. G. (2001) *Am. J. Physiol. Heart Circ. Physiol.* **281,** H2337–2365
21. Zaman, M. A., Oparil, S., and Calhoun, D. A. (2002) *Nat. Rev. Drug Discov.* **1,** 621–636
22. Harrison-Bernard, L. M., Navar, L. G., Ho, M. M., Vinson, G. P., and el-Dahr, S. S. (1997) *Am. J. Physiol.* **273,** F170–177
23. Miyata, N., Park, F., Li, X. F., and Cowley, A. W., Jr. (1999) *Am. J. Physiol.* **277,** F437–446
24. Ozono, R., Wang, Z. Q., Moore, A. F., Inagami, T., Siragy, H. M., and Carey, R. M. (1997) *Hypertension* **30,** 1238–1246
25. de Gasparo, M., Catt, K. J., Inagami, T., Wright, J. W., and Unger, T. (2000) *Pharmacol. Rev.* **52,** 415–472
26. Hunyady, L., and Catt, K. J. (2006) *Mol. Endocrinol.* **20,** 953–970
27. Bugaj, V., Pochynyuk, O., and Stockand, J. D. (2009) *Am. J. Physiol. Renal Physiol* **297,** F1411–1418
28. Pochynyuk, O., Bugaj, V., Rieg, T., Insel, P. A., Mironova, E., Vallon, V., and Stockand, J. D. (2008) *J. Biol. Chem.* **283,** 36599–36607
29. Pochynyuk, O., Rieg, T., Bugaj, V., Schroth, J., Fridman, A., Boss, G. R., Insel, P. A., Stockand, J. D., and Vallon, V. (2010) *FASEB J.* **24,** 2056–2065
30. Pochynyuk, O., Bugaj, V., Vandewalle, A., and Stockand, J. D. (2008) *Am. J. Physiol. Renal Physiol.* **294,** F38–46
31. Kemendy, A. E., Kleyman, T. R., and Eaton, D. C. (1992) *Am. J. Physiol.* **263,** C825–837
32. Gao, X., Wu, L., and O'Neil, R. G. (2003) *J. Biol. Chem.* **278,** 27129–27137
33. Wu, L., Gao, X., Brown, R. C., Heller, S., and O'Neil, R. G. (2007) *Am. J. Physiol. Renal Physiol.* **293,** F1699–1713
34. Jin, M., Wu, Z., Chen, L., Jaimes, J., Collins, D., Walters, E. T., and O'Neil, R. G. (2011) *PLoS One* **6,** e16713
35. Mamenko, M., Zaika, O., Jin, M., O'Neil, R. G., and Pochynyuk, O. (2011) *PLoS One* **6,** e22824
36. Staruschenko, A., Pochynyuk, O., Vandewalle, A., Bugaj, V., and Stockand, J. D. (2007) *J. Am. Soc. Nephrol.* **18,** 1652–1661
37. Levchenko, V., Zheleznova, N. N., Pavlov, T. S., Vandewalle, A., Wilson, P. D., and Staruschenko, A. (2010) *J. Cell. Physiol.* **223,** 252–259
38. Wang, T., and Giebisch, G. (1996) *Am. J. Physiol.* **271,** F143–149
39. Zaika, O., Mamenko, M., O'Neil, R. G., and Pochynyuk, O. (2011) *Am. J. Physiol. Renal Physiol.* **300,** F1105–1115
40. Wind, S., Beuerlein, K., Eucker, T., Müller, H., Scheurer, P., Armitage, M. E., Ho, H., Schmidt, H. H., and Wingler, K. (2010) *Br. J. Pharmacol.* **161,** 885–898
41. Butterworth, M. B., Frizzell, R. A., Johnson, J. P., Peters, K. W., and Edinger, R. S. (2005) *Am. J. Physiol. Renal Physiol.* **289,** F969–977
42. Braam, B., Mitchell, K. D., Fox, J., and Navar, L. G. (1993) *Am. J. Physiol.* **264,** F891–898
43. Navar, L. G., Prieto, M. C., Satou, R., and Kobori, H. (2011) *Curr. Opin. Pharmacol.* **11,** 180–186
44. Komlosi, P., Fuson, A. L., Fintha, A., Peti-Peterdi, J., Rosivall, L., Warnock, D. G., and Bell, P. D. (2003) *Hypertension* **42,** 195–199
45. Kobori, H., Nangaku, M., Navar, L. G., and Nishiyama, A. (2007) *Pharmacol. Rev.* **59,** 251–287
46. Kaschina, E., and Unger, T. (2003) *Blood Press.* **12,** 70–88
47. Wei, Y., Zavilowitz, B., Satlin, L. M., and Wang, W. H. (2007) *J. Biol. Chem.* **282,** 6455–6462
48. Yue, P., Sun, P., Lin, D. H., Pan, C., Xing, W., and Wang, W. (2011) *Kidney Int.* **79,** 423–431
49. Ma, H. P. (2011) *J. Biol. Chem.* **286,** 32444–32453
50. Brooks, H. L., Allred, A. J., Beutler, K. T., Coffman, T. M., and Knepper, M. A. (2002) *Hypertension* **39,** 470–473
51. Beutler, K. T., Masilamani, S., Turban, S., Nielsen, J., Brooks, H. L., Ageloff, S., Fenton, R. A., Packer, R. K., and Knepper, M. A. (2003) *Hypertension* **41,** 1143–1150